

# The impact of the carrier envelope phase – dependence on system and laser parameters

P.-G. Reinhard<sup>1</sup>, E. Suraud<sup>2</sup>, C. Meier<sup>3</sup>

<sup>1</sup> Institut für Theoretische Physik, Universität Erlangen, D-91058, Erlangen, Germany

<sup>2</sup> Laboratoire de Physique Théorique, Université de Toulouse, CNRS, UPS, France

<sup>3</sup> Laboratoire Collisions-Agrégats-Réactivité, Université de Toulouse, CNRS, UPS, France

E-mail: paul-gerhard.reinhard@physik.uni-erlangen.de

**Abstract.** We investigate, from a theoretical perspective, photo-emission of electrons induced by ultra-short infrared pulses covering only a few photon cycles. In particular, we investigate the impact of the Carrier-Envelope Phase (CEP) of the laser pulse which plays an increasingly large role for decreasing pulse length. As key observable we look at the asymmetry of the angular distribution as function of kinetic energy of the emitted electrons. The focus of the present study lies on the system dependence of the reaction. To this end, we study two very different systems in comparison, an Ar atom and the Na<sub>9</sub><sup>+</sup> cluster. The study employs a fully quantum-mechanical description of electron dynamics at the level of Time-Dependent Density Functional Theory (TDDFT). We find a sensitive dependence on the system which can be related to the different spectral response properties. Results can be understood from an interplay of the ponderomotive motion driven by the external photon field and dynamical polarization of the system.

PACS numbers: 31.15.ee, 31.15.es, 32.80.Fb, 32.80.Qk, 33.80.Eh

Submitted to: *J. Phys. B: At. Mol. Phys.*

## 1. Introduction

The enormous progress in laser technology has meanwhile reached the regime of extremely short pulses which cover only a few optical cycles [1, 2]. This opens the door to a great variety of new investigations such as time-resolved measurement of electronic processes or precision control of chemical reactions see, e.g., [3, 4, 5, 6, 7, 8, 9]. One of the main new aspects of such few-cycle pulses is that the Carrier Envelope Phase (CEP), i.e. the relative phase between the optical carrier wave and the pulse envelope, acquires a sensitive influence on the pulse shape which, in turn, can have a strong impact on all laser induced reactions [10, 11, 12]. This looks at first glance as a complication because there is one more laser parameter to be taken care of. But it can be turned into an advantage by potentially controlling electronic reactions with dedicated variations of

the CEP. A particularly interesting example is found in photo-electron emission where the CEP allows to control the forward-backward (also called “right-left”) asymmetry in the photo-electron spectra (PES) [13, 14]. Theoretical calculations have shown that the (high energy) parts of PES coming from electron recollisions are more sensitive to CEP than the (low energy) parts from directly emitted electrons [15, 12, 16, 17, 18]. Experimentally, the dependence of high-energy PES on the CEP has been explored for atoms [13, 19, 20], dimer molecules [21], and nano-tips [22, 23], providing challenging motivations for the theoretical investigations.

In a recent work, the Angular-Resolved PES (ARPES) of  $C_{60}$  were calculated as a function of the Carrier Envelope Phase (CEP) using a fully quantum-mechanical approach based on Time Dependent Density Functional Theory (TDDFT) and looking in particular at the asymmetry of the angular distribution for different kinetic energies of the emitted electrons [24]. These theoretical simulations allowed to reproduce the experimentally found dependencies on laser parameters, particularly on pulse length and CEP. The next question which comes up naturally is to which extend the results depend on the system which is irradiated. To answer this question, we have extended the previous calculations to include different atomic systems, notably atomic Argon and  $Na_9^+$  clusters. These systems were chosen, since they have about the same complexity (8 active electrons) but differ drastically in their electronic response: the photo-excitation spectrum of Ar has a discrete peak at about 15 eV followed by a widespread shoulder above while the spectrum of  $Na_9^+$  is dominated by a strong surface plasmon resonance at about 2.7 eV. It is obvious that an infrared (IR) laser is far closer to resonance for  $Na_9^+$  and this should have consequences. To investigate this in detail is the aim of the present work.

The paper is organized as follows: In section 2, we briefly review the theoretical framework. In section 3, we present and discuss the results.

## 2. Formal framework

We describe the electronic dynamics by Time-Dependent Density Functional Theory (TDDFT) at the level of the Time-Dependent Local Density Approximation (TDLDA) [25] using the exchange-correlation functional from [26]. For an appropriate modeling of electron emission, we augment the TDLDA by a Self-Interaction Correction (SIC) [27]. As a full SIC treatment is computationally very demanding, [28], we use it in a simplified, but reliable and efficient version as an Average Density SIC (ADSIC) [29]. The ADSIC is able to put the single-particle energies into the correct relation to the continuum threshold such that the ionization potential (IP) is properly reproduced in a great variety of systems [30]. A correct description of the IP is particularly important for the analysis of photoemission, the more so in connection with strong IR fields because here electrons in the highest occupied molecular orbitals dominate [31].

The ionic background is described by soft local pseudopotentials, for  $Na_9^+$  of Gaussian type [32] and for Ar using the functional form of [33]. The ions of  $Na_9^+$

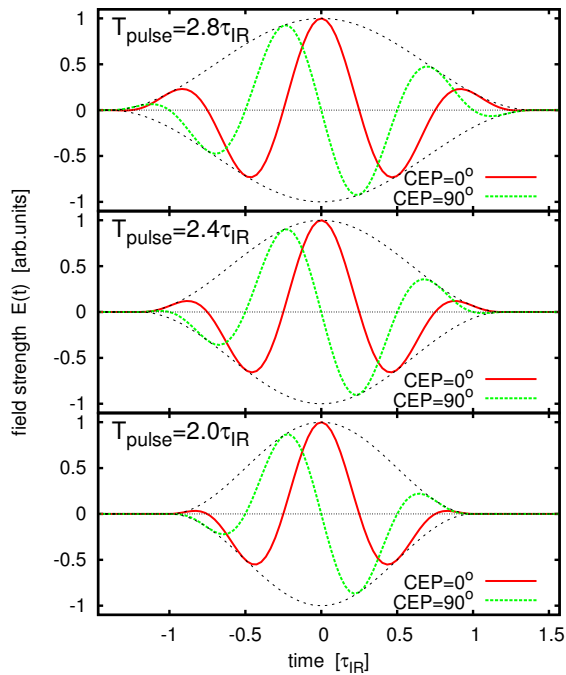


**Figure 1.** Examples of IR pulses for various pulse lengths  $T_{\text{pulse}}$  and two CEP as indicated. The dashed lines indicate the pulse envelope which does not depend on the CEP.

are kept frozen at the ground-state structure during the dynamical calculations. This is a legitimate approximation in view of the short laser pulses considered here.

The external, linearly polarized laser pulse is modeled within dipole approximation as the potential

$$v_{\text{las}}(\mathbf{r}, t) = -E(t) \mathbf{r} \cdot \mathbf{e}_z \quad (1a)$$

with the polarization vector along the  $z$ -axis  $\mathbf{e}_z$  and with the electric field

$$E(t) = E_0 \cos^2\left(\frac{\pi t}{T_{\text{pulse}}}\right) \cos(\omega_{\text{las}} t + \phi_{\text{CEP}}) \text{ for } -\frac{T_{\text{pulse}}}{2} \leq t \leq \frac{T_{\text{pulse}}}{2}. \quad (1b)$$

Here,  $E_0$  denotes the peak electric field,  $\omega_{\text{las}}$  the carrier frequency, and  $T_{\text{pulse}}$  the total pulse duration. The CEP is comprised in the parameter  $\phi_{\text{CEP}}$  which defines the phase between a maximum of oscillations with frequency  $\omega_{\text{las}}$  and the maximum of the  $\cos^2$  envelope. The minus sign in the definition of the potential guarantees that the driving force of the electrical field points in forward direction (positive  $z$ ) for positive field  $E(t)$ . In what follows, we use laser parameters close to those in recent experiments [34]: frequency  $\omega_{\text{las}} = 1.72$  eV (a wavelength of 720 nm), intensity  $I = 6 \times 10^{13}$  W/cm<sup>2</sup>, corresponding to field amplitude  $E_0 = 1.1$  eV/ $a_0$ , and total duration  $T_{\text{pulse}} = 4$  fs, 6 fs, and 8 fs, corresponding to 1.7, 2.5, and 3.3 optical cycles (1 optical cycle /  $\tau_{\text{IR}} = 2.4$  fs). Note that these laser parameters are associated with a ponderomotive energy  $U_p = 2.9$  eV. Figure 1 illustrates the temporal part of the laser field  $\propto E(t)$  for the three  $T_{\text{pulse}}$  under consideration, each one for the CEP at  $0^\circ$  and  $90^\circ$ . For  $\phi_{\text{CEP}} = 0^\circ$ , the center of the envelope (dashes) coincides with a maximum of the oscillations, while for  $\phi_{\text{CEP}} = 90^\circ$ , it is shifted to match with the nodal points of the electric field. Clearly, we see a substantial change of the electric field due to the different CEP in each case.

### 2.1. Numerical details

The TDLDA-ADSIC equations are solved numerically on a cylindrical grid in coordinate space [35]. The static iterations towards the electronic ground state are done with the damped gradient method [36] and the time evolution employs the time-splitting technique [37]. For details of the numerical method see [38, 39, 40]. We use a numerical box which extends to  $\pm 250 a_0$  in  $z$  direction (along the laser polarization) and  $250 a_0$  orthogonal to it (radial  $r$  coordinate), with a grid spacing of  $0.5 a_0$  in both directions. Time propagation is followed up to after 44 fs with a small time step of 1–5 attoseconds. Box size and time span are sufficiently large to track completely the rescattering of electrons in the laser field (ponderomotive motion). To account for ionization, absorbing boundary conditions are implemented using a mask function [41]. The absorbing margin extends over  $32 a_0$  at each side of the grid.

The central observable of electron emission in our analysis is the Angle-Resolved Photo-Electron Spectrum (ARPES), i.e., the yield of emitted electrons  $[\mathcal{Y}(E_{\text{kin}}, \theta)]$  as function of kinetic energy  $E_{\text{kin}}$  and emission angle  $\theta$ . We calculate an ARPES by recording at each time step the single-electron wave functions  $\{\psi_j(t, \mathbf{r}_{\mathcal{M}}), j = 1, \dots, N_{\text{el}}\}$  at selected measuring points  $\mathbf{r}_{\mathcal{M}}$  near the absorbing layer and finally transforming this information from time- to frequency-domain, see [42, 43, 44, 45]. Finally, the ARPES is written as

$$\mathcal{Y}(E_{\text{kin}}, \theta) \propto \sum_{j=1}^{N_{\text{el}}} |\widetilde{\psi}_j(E_{\text{kin}}, \mathbf{r}_{\mathcal{M}})|^2 \quad (2)$$

where  $\widetilde{\psi}_j$  are the transformed wave functions in energy domain. In case of strong fields, as we encounter here, the  $\widetilde{\psi}_j$  are augmented by a phase factor accounting for the ponderomotive motion, for technical details see [44]. The angle  $\theta$  is defined with respect to  $\mathbf{e}_z$ , i.e.  $\theta = 0^\circ$  means electronic emission in the direction of  $\mathbf{e}_z$ . A detailed ARPES analysis requires a fine resolution for Fourier transformation and emission angles. To that end, we use an increment of 0.04 eV in energy and  $1^\circ$  opening angle for the angular bins.

It is cumbersome and confusing to check the full ARPES for all variations of laser parameters. It turns out that a key feature is the asymmetry of the angular distribution

$$\eta = \frac{Y_+(E_{\text{kin}}, \Theta) - Y_-(E_{\text{kin}}, \Theta)}{Y_+(E_{\text{kin}}, \Theta) + Y_-(E_{\text{kin}}, \Theta)}, \quad (3a)$$

$$Y_+(E_{\text{kin}}, \Theta) = \int_0^\Theta d\theta \mathcal{Y}(E_{\text{kin}}, \theta) \quad (3b)$$

$$Y_-(E_{\text{kin}}, \Theta) = \int_{180^\circ - \Theta}^{180^\circ} d\theta \mathcal{Y}(E_{\text{kin}}, \theta) \quad (3c)$$

which is a function of kinetic energy  $E_{\text{kin}}$  and opening angle  $\Theta$  over which angular averaging is done. In most experiments, photoelectron yields are collected in a cone angle of  $\Theta = 15^\circ$ . Thus we are using this value throughout and will not indicate this

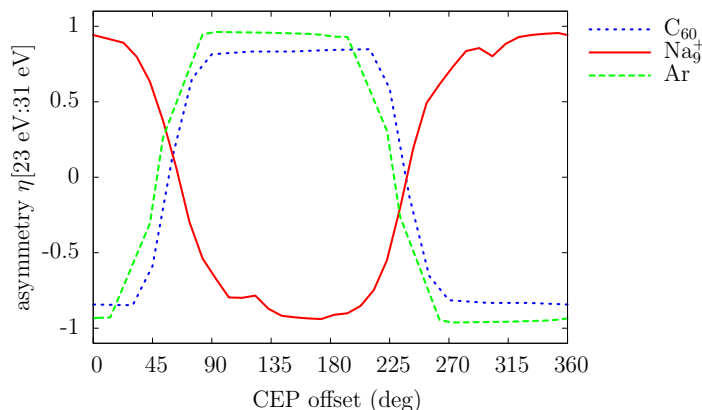


**Figure 2.** Integrated asymmetry parameter  $\eta[23\text{eV} : 31\text{eV}]$  for three different systems:  $\text{C}_{60}$  cluster,  $\text{Ar}$  atom, and  $\text{Na}_9^+$  cluster. Laser parameters were: frequency  $\omega_{\text{las}} = 1.72 \text{ eV}$ , intensity  $I_{\text{las}} = 6 \times 10^{13} \text{ W/cm}^2$  corresponding to field strength  $E_0 = 1.1 \text{ eV/a}_0$ , and pulse length  $T_{\text{pulse}} = 6 \text{ fs}$  (corresponding to 2.5 IR cycles).

dependence any more. Of course, this  $\eta$  depends on more parameters, particularly on all laser parameters. We will in the following look particularly at the dependence on the CEP.

In some cases, we compress the information by integrating over certain energy bands. This yields a more compact asymmetry parameter

$$\eta[E_1 : E_2] = \frac{\tilde{Y}_+[E_1 : E_2] - \tilde{Y}_-[E_1 : E_2]}{\tilde{Y}_+[E_1 : E_2] + \tilde{Y}_-[E_1 : E_2]} \quad , \quad (4)$$

$$\tilde{Y}_{\pm}[E_1 : E_2] = \int_{E_1}^{E_2} dE_{\text{kin}} Y_{\pm}(E_{\text{kin}}, 15^\circ) \quad , \quad (5)$$

where we use the same symbol  $\eta$  and distinguish by indicating its dependencies.

### 3. Results

#### 3.1. Introductory example

For a first comparison of systems, we chose the integrated asymmetry Eq. (4) versus CEP as simple signal. Results for three different systems are compared in figure 2: the  $\text{C}_{60}$  cluster to establish the link to the previous study [24], the  $\text{Ar}$  atom, and the  $\text{Na}_9^+$  cluster. The first two samples,  $\text{C}_{60}$  and  $\text{Ar}$ , show a very similar behavior and one is tempted to expect a generic signal formed only by laser properties. However, the  $\text{Na}_9^+$  cluster yields a CEP dependence with exactly opposite pattern which clearly demonstrates a strong impact of the electronic system. The difference between  $\text{Ar}$  and  $\text{Na}_9^+$  suggests naturally a relation to their much different spectral response. This assumption is, in fact, confirmed by the case of  $\text{C}_{60}$ . Although this large cluster is structurally much different from the  $\text{Ar}$  atom the spectral relations are similar to  $\text{Ar}$  in that the dipole strength lies far above the IR frequency and is rather fragmented. We shall thus continue our investigations keeping only  $\text{Ar}$  and  $\text{Na}_9^+$  for the sake of simplicity.

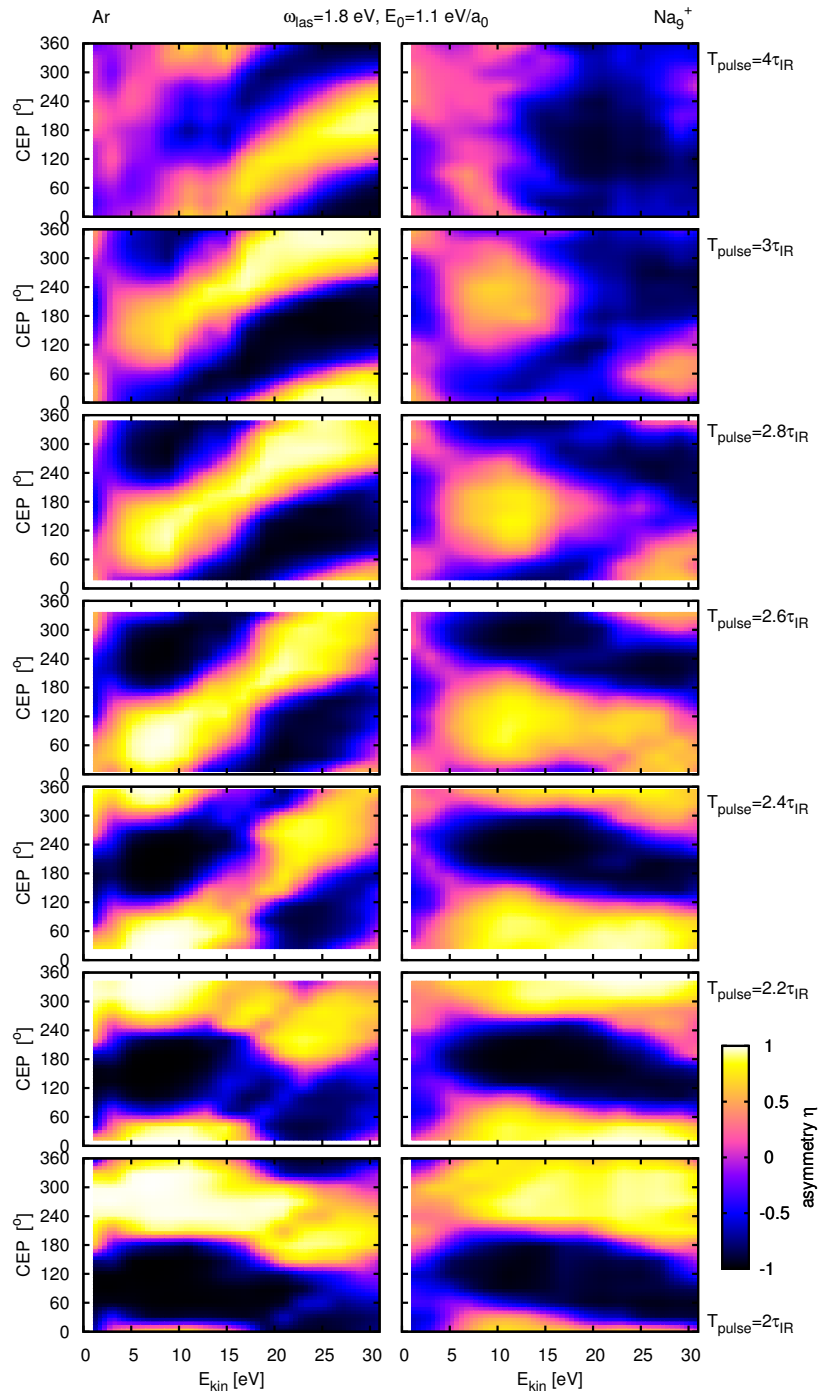


**Figure 3.** Asymmetry  $\eta$  in the plane of kinetic energy and CEP for  $\omega_{\text{las}} = 1.8$  eV,  $E_0 = 1.1$  eV/ $a_0$ , and different pulse lengths as indicated.

### 3.2. Comparison of Ar atom and $\text{Na}_9^+$ cluster

In this section, the simultaneous dependence of the asymmetry parameter  $\eta$  on the CEP and the kinetic energy  $E_{\text{kin}}$  of emitted electrons is analyzed in detail. The results of this 3D information are presented as a color map. Figure 3 shows a series of results for

different pulse lengths  $T_{\text{pulse}}$ . Let us first look at extremely short pulses,  $T_{\text{pulse}} = 2\tau_{\text{IR}}$ , i.e. practically less than two optical cycles because of the the profile shape (see Fig. 1). Here, the CEP dependence of the asymmetry is very similar for both systems (Ar and  $\text{Na}_9^+$ ) and the asymmetry is more or less the same over the whole range of  $E_{\text{kin}}$ . The independence from the system is plausible because very short pulses give the system little chance to develop its dynamical response such that the shape of the external laser pulse dominates the process and this is the same in all systems. The independence from the CEP is also plausible because too short pulses have basically one or two dominating peaks which gives little chances for ponderomotive effects which otherwise can produce a difference between low-energy and high-energy emission [24]. The emission maxima (corresponding to  $\eta \sim \pm 1$ ) lie at  $\phi_{\text{CEP}} = 90^\circ$  and  $\phi_{\text{CEP}} = 270^\circ$ . These are the situations where exactly two equally strong peaks compete and the preferred direction of emission coincides with the direction of the second peak. For example, the second of the large peaks points to negative  $z$  for  $\phi_{\text{CEP}} = 90^\circ$ , see Fig. 1, and so backward emission ( $\eta \approx -1$ ) prevails. This agrees with the analysis of detailed time dependence in section 3.3 which shows that the emission from earlier peaks is practically pushed back by the subsequent counter-peaks and that emission from the last peak experiences least hindrance.

However, when slightly longer pulses are considered, the picture changes. Directly above  $T_{\text{pulse}} = 2\tau_{\text{IR}}$  comes a region where pattern change quickly and the difference between Ar and  $\text{Na}_9^+$  develops. Already at  $T_{\text{pulse}} = 2.4\tau_{\text{IR}}$  we can see a striking difference between the patterns for Ar and  $\text{Na}_9^+$ : while in the case of  $\text{Na}_9^+$ , (right panel), the asymmetry has not changed significantly as compared to  $T_{\text{pulse}} = 2.0\tau_{\text{IR}}$ , the asymmetry has developed a clear energy dependence for Ar. In the latter case, the asymmetry in the low-energy and high-energy ranges show opposite behavior: for instance, for  $\phi_{\text{CEP}} = 240^\circ$ , low energy electrons ( $\approx 5\text{--}10$  eV) are mainly emitted in forward direction, while high energy electrons  $\approx 22$  eV backward. The reason for this behavior lies in the optical properties of the field and the electronic response: for a pulse duration of  $T = 2.4\tau_{\text{IR}}$ , the electric field explores already a bit more oscillations which enhances the playground for ponderomotive motion and this, in turn, gives the high-energy electron a different emission dynamics. This behavior is similar to the one found in  $\text{C}_{60}$  previously and discussed in [24]. One then wonders why this does not happen in the same manner for  $\text{Na}_9^+$ . The key point is here that the external driving field and the dipole response run out of phase due to the impact of the strong plasmon resonance. This interferes with the mechanism worked out for Ar and  $\text{C}_{60}$ . In section 3.3, the difference in dynamical behaviors will be analyzed based on the detailed time evolution of electron density.

Finally, when going to even longer pulses, the asymmetry vanishes altogether. The reason for this behavior is obvious. Longer pulses contain more optical cycles, the individual peaks of the electric field that point into opposite directions with nearly equal strength and the CEP does not make much of a difference any more. It is interesting, however, that the smoothing of asymmetry pattern as a function of CEP starts for  $\text{Na}_9^+$  already at  $T_{\text{pulse}} = 3\tau_{\text{IR}}$  while it takes up to much larger  $T_{\text{pulse}}$  to reach that stage for Ar. The reason is, again, the different optical response. The interference of external

frequency and resonance frequency in the dipole response of  $\text{Na}_9^+$  perturbs the emission process and so spoils CEP dependence earlier.

### 3.3. Time evolution in detail

In order to get a deeper insight into emission direction, we analyze the time evolution of electron density for a pulse length in the critical regime,  $T_{\text{pulse}} = 2.6\tau_{\text{IR}}$ , and here for  $\phi_{\text{CEP}} = 270^\circ$  where the difference between Ar and  $\text{Na}_9^+$  is most marked.

The lower panel of figure 4 shows the densities for Ar and  $\text{Na}_9^+$  as 3D color map plot. This is complemented by the full ARPES in the upper panel and time evolution of external field together with volume dipole moment in the middle panel. The notion of a “volume dipole” requires an explanation. The normal dipole moment  $d = \int d^3r z \rho$  is blurred by pieces of emitted electronic density far away from the system, i.e. at large  $z$ . However, we are interested on a signal from the bulk density at the system. In order to focus on the regions of high density, we consider the  $z$  moment of  $\rho^2$ , i.e.  $d^{(2)} = \int d^3r z \rho^2$ , which we call volume dipole because it emphasizes the volume rather than the surface.

The ARPES in the upper panel illustrates how the asymmetry pattern (see figure 3) are generated. For Ar, we see a preference of backward emission (angle  $180^\circ$ ) at energies around 5 eV turning to a bias on backward emission for higher energies  $> 20$  eV while for  $\text{Na}_9^+$  backward emission prevails in the whole range (except for very low energies  $< 2$  eV), in accordance with the panel for  $T_{\text{pulse}} = 2.6\tau_{\text{IR}}$  in figure 3.

Dipole and field signals in the middle panel illustrate nicely the dramatic differences in the systems response. Already the dipole amplitude for Ar is much smaller than for  $\text{Na}_9^+$  which indicates that Ar is a much less responsive system. This off-resonant behavior for Ar is also visible from the fact that the dipole signal follows the external field in phase. There are small, fast oscillations super-imposed in the dipole signal which stem from a small excitation of systems frequencies. The  $\text{Na}_9^+$  cluster behaves much differently. Here we see already in the first oscillation a large phase shift of dipole versus external field. The shift changes along the signal. It seems that the dipole response has a trend to oscillate with the faster plasmon frequency rather than those of the external field. Mind that emission is driven by the dipole moment whereas propagation of the emitted electron follows the external field. These two ingredients now run at different pace for  $\text{Na}_9^+$  producing a subtle interplay of driving forces. The trends thus can go in any direction and it requires detailed modeling to make predictions for such highly reactive systems.

Finally, the lower panel of figure 4 shows the time evolution of electron density along  $z$  axis (laser polarization axis). Logarithmic scale is chosen to visualize the outer tail of the electron distribution which represents electron emission. In the first 3 fs, we see outbursts of electrons which are, however, turned back to the center. Consider the first bump toward negative  $z$ . This outflow is triggered by the first peak of  $E(t)$ , or  $d^{(2)}(T)$  respectively. It moves on until the opposite peak in field strengths pushes it back

to the center. The same happens with electrons emitted through the second (positive) peak in direction of positive  $z$ . Here the counter-force in negative direction does not complete its job and part of the backflow merges with the outgoing wave from the second positive peak. The waves finally reaching the boundaries stem all from the latest peaks of the pulse which are not counter-weighted by subsequent opposite peaks. The final outflow mixes electrons which are directly emitted with those which have gained more

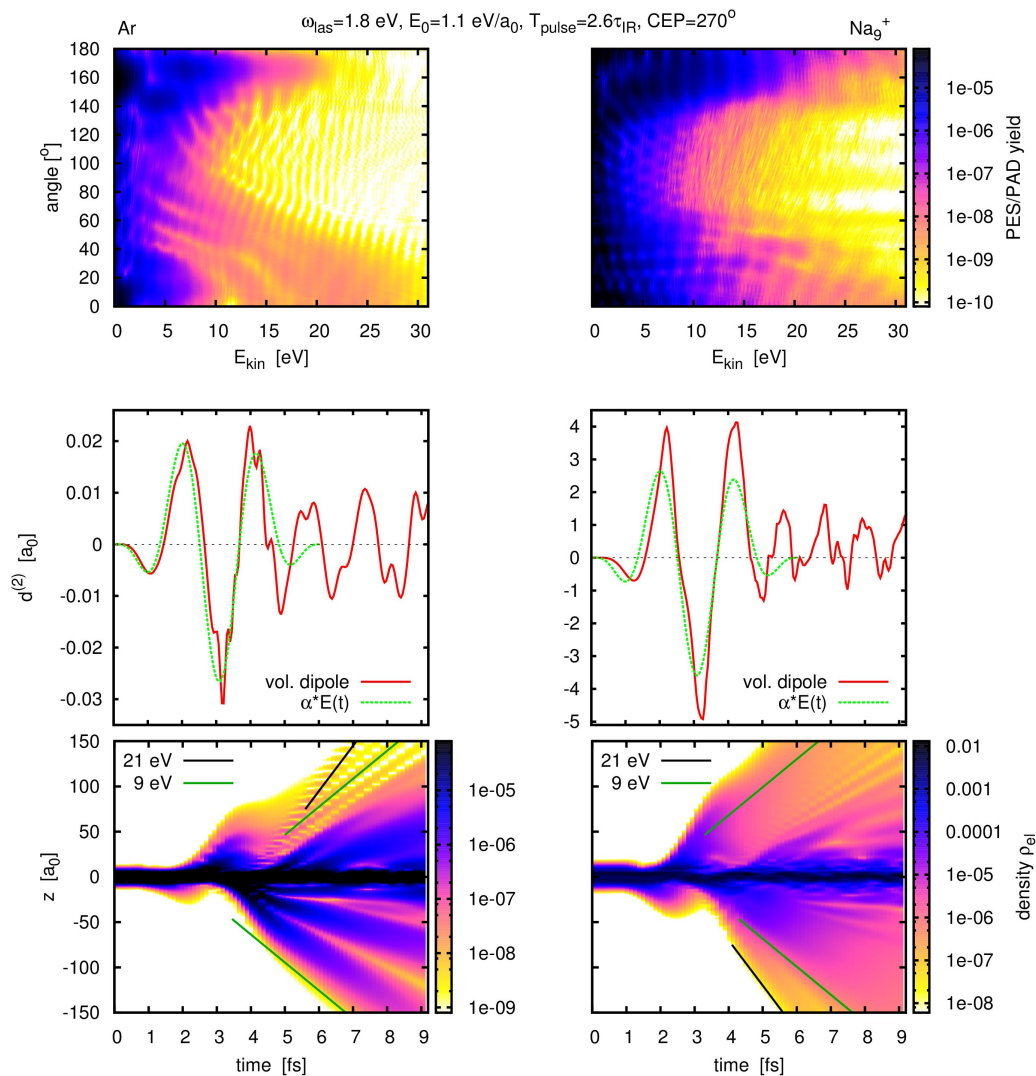


**Figure 4.** Analysis of the case  $\omega_{\text{las}} = 1.8$  eV,  $E_0 = 1.1$  eV/a<sub>0</sub>, pulse length  $T_{\text{pulse}} = 2.6\tau_{\text{IR}}$ , and CEP=270° for Ar (left) and Na<sub>9</sub><sup>+</sup> (right). Upper: ARPES yield  $\mathcal{Y}$  in the plane of kinetic energy  $E_{\text{kin}}$  and emission angle  $\theta$ . Middle: external field and volume dipole  $d^{(2)} = \int d^3r z \rho^2 / \int d^3r \rho^2$  as function of time. The external field is scaled such that the first maximum matches with the dipole. The scaling factor is  $\alpha = 0.025a_0^2/\text{eV}$  for Ar and  $\alpha = 3.3a_0^2/\text{eV}$  for Na<sub>9</sub><sup>+</sup>. Lower: Density (in logarithmic color scale) in the plane of time and  $z$ -coordinate. The black lines indicate the slope of a point moving with  $E_{\text{kin}} = 21$  eV, typical for the high-energy regime, and the green lines indicate  $E_{\text{kin}} = 9$  eV, typical for the low-energy regime.

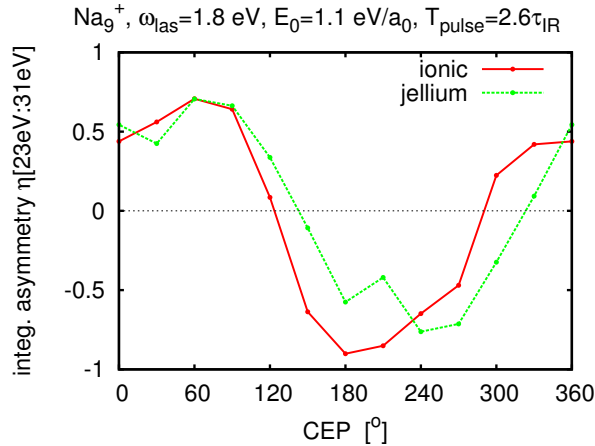


**Figure 5.** Integrated asymmetry  $\eta[23\text{eV} : 31\text{eV}]$  versus CEP comparing results from ionic background with jellium background. Laser parameters were:  $\omega_{\text{las}} = 1.8$  eV,  $E_0 = 1.1$  eV/a<sub>0</sub>, and  $T_{\text{pulse}} = \tau_{\text{IR}}$ .

energy by rescattering processes. This is indicated by the lines drawn into the plot. The black lines visualize flow with a high kinetic energy of 21 eV and the green ones with a low kinetic energy of 9 eV. For Ar, the dominance of the external field over the dipole response (mind the scaling in the left middle panel) enhances the ponderomotive effects and thus the high-energy electrons can only escape after the last peak, thus in forward direction. For Na<sub>9</sub><sup>+</sup>, on the other hand, the external field is considerably weaker which allows high-energy electrons to escape already the second last peak pointing in negative direction. This, however, should not be taken as general rule. The subtle interplay of drivers in Na<sub>9</sub><sup>+</sup> inhibits simple estimates.

### 3.4. Impact of the systems geometry

To check the effect of ionic background, we compare in figure 5 results from a calculation with ionic background with one using a soft jellium background [39]. We use for the jellium parameters a Wigner-Seitz radius of  $r_s = 3.65a_0$  and surface thickness of  $1a_0$  to place the surface plasmon resonance at similar spectral position as for the case of ionic background. The pulse length is chosen in the critical regime to explore most sensitivity to system parameters. The results are qualitatively the same. There are, of course, differences in detail. But these could very well be due to the slightly different spectral properties of the two systems. We can safely conclude that details of the background structure do not matter much for the structure of ARPES at these (low) laser frequencies. Note, however, that a sensitivity to ionic detail develops for laser pulses with higher frequencies and was found in earlier studies on angular distributions [46].

### 3.5. Impact of laser parameters

So far, we have considered laser pulses with frequency and intensity close to the experimental conditions of former studies in C<sub>60</sub>. It is, of course, interesting to check the influence of laser parameters. We do that here for the case of Na<sub>9</sub><sup>+</sup>. Figure 6 shows

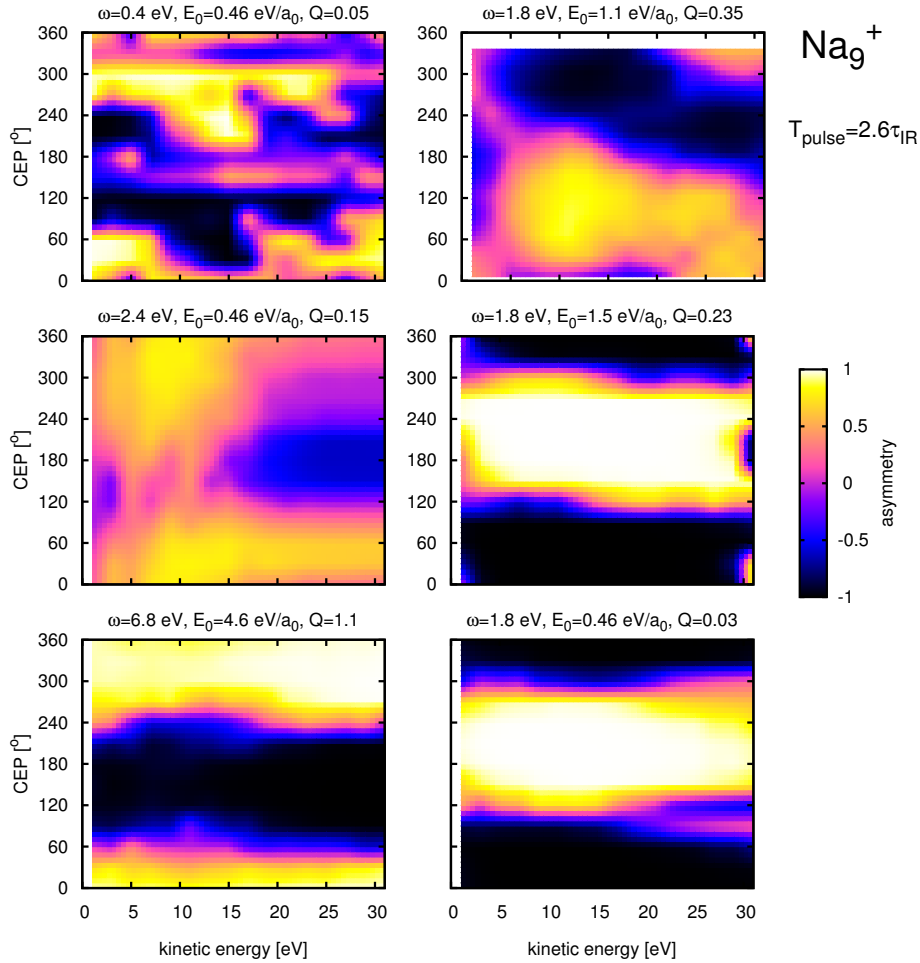


**Figure 6.** Asymmetry  $\eta$  in the plane of kinetic energy and CEP for  $\text{Na}_9^+$ ,  $T_{\text{pulse}} = 2.6\tau_{\text{IR}}$ , and various laser parameters as indicated. Together with the laser parameters, we also provide the total ionization  $Q$  induced by laser excitation.

the asymmetry  $\eta$  in the plane of kinetic energy and CEP for  $\text{Na}_9^+$  and a variety of laser frequencies and intensities. The left panels collect variation of frequency and the right panels variation of field strength (for fixed frequency  $\omega_{\text{las}} = 1.8 \text{ eV}$ ). Pulse length is  $T_{\text{pulse}} = 2.6\tau_{\text{IR}}$ , the same in all cases. The pattern differ dramatically for the different laser conditions. Let us try to give an interpretation to each case in the light of what we have learned above.

The left column collects variation of frequency. The high-frequency case (lower left panel) shows no energy dependence at all. This reminds the field dominated case of short pulses in figure 3 and, in fact, we encounter here a similar situation. At an absolute scale, the pulses are extremely short thus overruling any system response. The resonant case (middle left panel) at surface plasmon frequency looks somewhat blurred resembling the cases with longer pulses in figure 3. Indeed, we deal effectively with a long pulse because the resonant excitation induces dipole oscillations which carry on long after the external field has been turned off. The extremely low frequency (upper left panel) moves the

photon field well out of resonance, similar as the IR field was off resonance for Ar. But the pattern do not show the regular trends as in case of Ar. The quasi-static field at this extremely low frequency creates a very special situation. Although field strength seems weak, the long time a certain pulling force persists leads to large ponderomotive excursions. This together with a small amount of comparatively much faster plasmon oscillations generates these sort of chaotic, quickly changing asymmetries.

The right column of figure 6 collects variation of field strength. The upper right panel repeats the reference case which we had studied before in detail. Lower field strength (middle and lower right panels) reduce the ponderomotive effects even further and so diminish the differences between high-energy and low-energy electrons. What remains is pronounced forward emission for CEP  $0^\circ$  following the strongest peak in that case and correspondingly pronounced backward emission for  $180^\circ$ .

#### 4. Conclusion

In continuation of a previous study on  $C_{60}$ , we have investigated the system dependence of the impact of the carrier-envelope phase (CEP) of few-cycle laser pulses using as two very different systems an Ar atom and a  $Na_9^+$  cluster. As theoretical tool for this survey we use time-dependent density functional theory using standard local energy-density functionals. A self-interaction correction is added to achieve a correct dynamical description of emission properties. As in previous experimental and theoretical studies, we take as key observable the detailed electronic emission properties in angular resolved photo-electron spectra (ARPES). The angular information is compressed to the asymmetry of the angular distribution as function of energy which yields a compact measure well suited for a survey of varying conditions.

The two systems under consideration differ dramatically in their spectral properties. The Ar atom has a rather rigid dipole response with the first excitations lying high above IR frequencies. In this respect, the Ar atom is similar to the  $C_{60}$  cluster. Although the latter has a much more complex background structure the results for asymmetry as function of CEP are practically the same for these both systems. Quite differently, the  $Na_9^+$  cluster has a large polarizability and its spectrum is dominated by the strong surface plasmon resonance in the visible range, above IR frequencies but not too far away. In consequence, the results for ARPES from few cycle pulses differ dramatically from those of the Ar atom. By looking at the time evolution of density in detail, this difference could be clearly related to the different dynamical polarizability. The dipole moment of Ar follows the external field without delay whereas for  $Na_9^+$  it starts with a sizable phase shift from the onset and develops further phase deviations in the course of dynamics. This produces a much different interplay between electron emission, triggered by the dipole moment, and subsequent ponderomotive motion, governed by the external field. The more involved interplay between dipole and external field in case of  $Na_9^+$  hinders to develop simple predictions. A full simulation taking into account properly the dynamical response of a system is necessary.

Concerning variation of laser parameters, the length of the pulse plays a key role for the impact of the CEP. Longer pulses covering several optical cycles render the CEP unimportant. Very short pulses, up to 2 cycles, reduce the impact of the systems response and let the effects of external field dominate. In between comes a transitional region where the CEP dependence of ARPES changes quickly and becomes extremely system dependent. We also checked the influence of the other laser parameters for the more responsive system  $\text{Na}_9^+$  in the critical, transitional regime of pulse lengths and find, not surprisingly, a sensitive dependence to any parameter. The qualitative structure of the results can be explained in each case by the relative importance of ponderomotive motion in the external field and dipole response of the system.

Acknowledgment:

We thank the regional computing center of the university Erlangen-Nürnberg for generous supply of computer time for the demanding calculations. The work was supported by the Institut Universitaire de France and a French ANR contract LASCAR (ANR-13-BS04-0007).

- [1] Nisoli M, De Silvestri S, Svelto O, Szipöcs R, Ferencz K, Spielmann C, Sartania S and Krausz F 1997 *Opt. Lett.* **22** 522
- [2] Brabec T and Krausz F 2000 *Rev. Mod. Phys.* **72** 545
- [3] Baltuška A, Udem T, Uiberacker M, Hentschel M, Goulielmakis E, Gohle C, Holzwarth R, Yakovlev V, Scrinzi A, Hänsch T *et al.* 2003 *Nature* **421** 611
- [4] Kling M, Siedschlag C, Verhoef A J, Khan J, Schultze M, Uphues T, Ni Y, Uiberacker M, Drescher M, Krausz F *et al.* 2006 *Science* **312** 246
- [5] Milošević D, Paulus G G, Bauer D and Becker W 2006 *J. Phys. B: At. Mol. Opt. Phys.* **39** R203
- [6] Haessler S, Caillat J and Salieres P 2011 *J. Phys. B: At. Mol. Opt. Phys.* **44** 203001
- [7] Liu Y, Liu X, Deng Y, Wu C, Jiang H and Gong Q 2011 *Phys. Rev. Lett.* **106**(7) 073004
- [8] Krüger M, Schenk M, Förster M and Hommelhoff P 2012 *J. Phys. B: At. Mol. Opt. Phys.* **45** 074006
- [9] Xie X, Doblhoff-Dier K, Roither S, Schöffler M S, Kartashov D, Xu H, Rathje T, Paulus G G, Baltuška A, Gräfe S and Kitzler M 2012 *Phys. Rev. Lett.* **109**(24) 243001
- [10] Tempea G, Geissler M and Brabec T 1999 *JOSA B* **16** 669
- [11] Paulus G G, Grasbon F, Walther H, Villoresi P, Nisoli M, Stagira S, Priori E and De Silvestri S 2001 *Nature* **414** 182
- [12] Chelkowski S and Bandrauk A D 2005 *Phys. Rev. A* **71** 053815
- [13] Paulus G G, Lindner F, Walther H, Baltuška A, Goulielmakis E, Lezius M and Krausz F 2003 *Phys. Rev. Lett.* **91**(25) 253004
- [14] Corkum P B 1993 *Phys. Rev. Lett.* **71** 1994
- [15] Milošević D, Paulus G G and Becker W 2003 *Opt. Express* **11** 1418
- [16] Tong X M, Hino K and Toshima N 2006 *Phys. Rev. A* **74**(3) 031405
- [17] Liao Q, Lu P, Lan P, Cao W and Li Y 2008 *Phys. Rev. A* **77**(1) 013408
- [18] Suárez N, Chacón A, Ciappina M F, Biegert J and Lewenstein M 2015 *Phys. Rev. A* **92** 063421
- [19] Lindner F, Schätzel M G, Walther H, Baltuška A, Goulielmakis E, Krausz F, Milošević D B, Bauer D, Becker W and Paulus G G 2005 *Phys. Rev. Lett.* **95**(4) 040401
- [20] Kling M, Rauschenberger J, Verhoef A, Hasović E, Uphues T, Milošević D, Muller H and Vrakking M 2008 *New J. Phys.* **10** 025024
- [21] Gazibegović-Busuladžić A, Hasović E, Busuladžić M, Milošević D B, Kelkensberg F, Siu W K, Vrakking M J J, Lépine F, Sansone G, Nisoli M, Znakovskaya I and Kling M F 2011 *Phys. Rev. A* **84**(4) 043426

- [22] Krüger M, Schenk M and Hommelhoff P 2011 *Nature* **475** 78
- [23] Park D J, Piglosiewicz B, Schmidt S, Kollmann H, Mascheck M and Lienau C 2012 *Phys. Rev. Lett.* **109**(24) 244803
- [24] Gao C Z, Dinh P M, Reinhard P G, Suraud E and Meier C 2017 *Phys. Rev. A* **95** 033427
- [25] Dreizler R M and Gross E K U 1990 *Density Functional Theory: An Approach to the Quantum Many-Body Problem* (Berlin: Springer-Verlag)
- [26] Perdew J P and Wang Y 1992 *Phys. Rev. B* **45** 13244
- [27] Perdew J P and Zunger A 1981 *Phys. Rev. B* **23** 5048
- [28] Messud J, Dinh P M, Reinhard P G and Suraud E 2008 *Ann. Phys. (N.Y.)* **324** 955
- [29] Legrand C, Suraud E and Reinhard P G 2002 *J. Phys. B: At. Mol. Opt. Phys.* **35** 1115
- [30] Klüpfel P, Dinh P M, Reinhard P G and Suraud E 2013 *Phys. Rev. A* **88** 052501
- [31] Müller H G and Fedorov M 1996 *Super-intense laser-atom physics IV* vol 13 (Springer Science & Business Media)
- [32] Kümmel S, Brack M and Reinhard P G 2000 *Phys. Rev. B* **62** 7602
- [33] Goedecker S, Teter M and Hutter J 1996 *Phys. Rev. B* **54** 1703
- [34] Li H, Mignolet B, Wachter G, Skruszewicz S, Zhrebtsov S, Süßmann F, Kessel A, Trushin S, Kling N G, Kübel M *et al.* 2015 *Phys. Rev. Lett.* **114**(12) 123004
- [35] Montag B and Reinhard P G 1995 *Z. Phys. D: At., Mol. Clusters* **33** 265
- [36] Reinhard P G and Cusson R 1982 *Nucl. Phys. A* **378** 418
- [37] Feit M, Fleck J and Steiger A 1982 *J. Comput. Phys.* **47** 412
- [38] Calvayrac F, Reinhard P G, Suraud E and Ullrich C A 2000 *Phys. Rep.* **337** 493
- [39] Reinhard P G and Suraud E 2003 *Introduction to Cluster Dynamics* (New York: Wiley)
- [40] Wopperer P, Dinh P M, Reinhard P G and Suraud E 2015 *Phys. Rep.* **562** 1
- [41] Reinhard P G, Stevenson P D, Almehed D, Maruhn J A and Strayer M R 2006 *Phys. Rev. E* **73** 036709
- [42] Pohl A, Reinhard P G and Suraud E 2001 *J. Phys. B* **34** 4969
- [43] De Giovannini U, Varsano D, Marques M A L, Appel H, Gross E K U and Rubio A 2012 *Phys. Rev. A* **85**(6) 062515
- [44] Dinh P M, Romaniello P, Reinhard P G and Suraud E 2013 *Phys. Rev. A* **87** 032514
- [45] Dauth M and Kümmel S 2016 *Phys. Rev. A* **93**(2) 022502
- [46] Pohl A, Reinhard P G and Suraud E 2004 *Phys. Rev. A* **70** 023202